

Ground support performance in deep underground mine with large anisotropic deformation using calibrated numerical simulation (case of mine-H)

Bo Hu^{1,6}, Mostafa Sharifzadeh^{*2,3}, Xia-Ting Feng³, Roo Talebi⁴ and Jin-Fu Lou⁵

¹School of Civil Engineering, Chongqing Jiaotong University, Chongqing 400074, China

²Department of Mining Engineering, Western Australian School of Mines, Curtin University, Kalgoorlie 6430, Australia

³Key Laboratory of Ministry of Education on Safe Mining of Deep Metal Mines, Northeastern University, Shenyang 110819, China

⁴Northern Star Resources Ltd, Kalgoorlie WA 6430, Australia

⁵Mining and Designing Branch, China Coal Research Institute, Beijing, China

⁶Inner Mongolia Key Laboratory of Mining Pressure and Strata Control, Hulunbeir University, Hulunbeir 021008, China

(Received December 2, 2019, Revised April 12, 2020, Accepted May 16, 2020)

Abstract. High-stress and complex geological conditions impose great challenges to maintain excavation stability during deep underground mining. In this research, large anisotropic deformation and its management by support system at a deep underground mine in Western Australia were simulated through three-dimensional finite-difference model. The ubiquitous-joint model was used and calibrated in FLAC3D to reproduce the deformation and failure characteristics of the excavation based on the field monitoring results. After modeling verification, the roles of mining depth also the intercept angle between excavation axis and foliation orientation on the deformation and damage were studied. Based on the results, quantitative relationships between key factors and damage classifications were presented, which can be used as an engineering tool. Subsequently, the performance of support system installation sequences was simulated and compared at four different scenarios. The results show that, first surface support and then reinforcement installation can obtain a better controlling effect. Finally, the influence of bolt spacing and ring spacing were also discussed. The outcomes obtained in this research may play a meaningful reference for facing the challenges in thin-bedded or foliated ground conditions.

Keywords: large deformation; squeezing; intercept angle; ground reinforcement; ubiquitous-joint model; support standard

1. Introduction

As mining depth extends to deep underground, high-stress concentration or mining-induced stresses becomes much severe. Different cross-section closure magnitudes can be induced by the high-stress environment and squeezing phenomenon becomes more frequent. When encountering the jointed ground, significant convergence and anisotropic phenomenon can be observed as illustrated in Fig. 1. These potential factors induce large anisotropic deformation, support elements failure and even machinery trapping which needs rehabilitation. As a result, the normal mining production will be delayed and can jeopardize safety. Maintaining the stability of the excavation in foliated ground brings a great challenge for geotechnical engineers. During underground mining production, a common and easy method to monitor the deformation is the wall-to-wall or back-to-floor convergence which can also be used to calculate the closure strain by dividing the deformation to the original size of the excavation. The excavation deformation highly depends on the ground geology and stress conditions (Meguid and Rowe 2006, Aksoy *et al.* 2020, Wu *et al.* 2019a, b and 2020). The foliation structures

around the excavation induce significant anisotropy especially for the spatial relationship between the excavation direction and the joint orientation (Kolymbas *et al.* 2006, Vu *et al.* 2013, Schubert and Mendez 2017). Based on the laboratory tests, the rock strength shows significant anisotropic characteristic which depends on the loading direction to the foliation orientation (Bagheripour *et al.* 2011, Watson *et al.* 2015). As a result, the failure mechanisms of the excavations in foliated ground is mainly divided into shearing, bulking, buckling and sliding-bending (Sandy 2010, Kazakidis 2002). An extensive investigation shows that there are two direct factors affecting on the anisotropic deformation of the excavation in the jointed ground such as mining depth and the relative intercept angle between the excavation axis and foliation orientation. Deep mining is often constrained by high stresses. The anisotropic foliated or thin-bedded rock masses cause many problems for controlling surrounding rocks. For instance, there are a lot of rock mines excavated in the deep jointed ground in Australia, Canada and South Africa where shows typical squeezing conditions (Stephenson and Sandy 2017). Controlling the large anisotropic deformation of the ore drives faces significant challenge (Sandy *et al.* 2007, Karampinos and Hadjigeorgiou *et al.* 2017). Therefore, it is necessary to investigate the large anisotropic deformation of the excavation and corresponding controlling strategy.

*Corresponding author, Professor
E-mail: m.sharifzadeh@curtin.edu.au

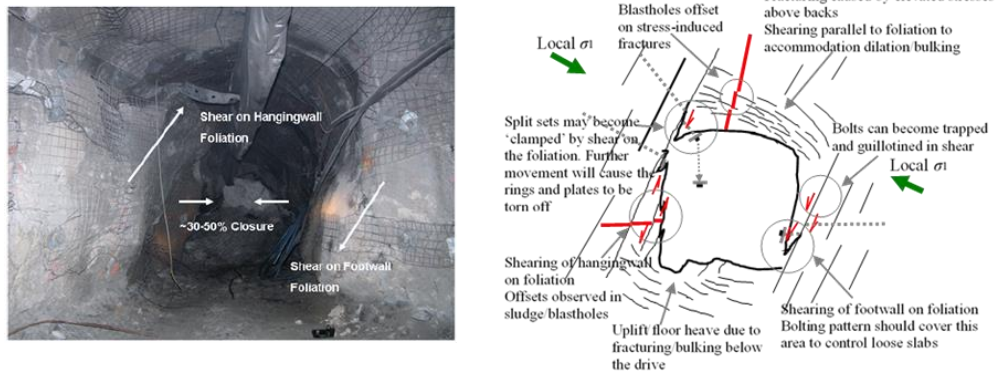


Fig. 1 Typical large deformation of the excavation in foliated ground and schematic diagram of the failure mechanism (Modified after Sandy *et al.* 2007)

Appropriate support systems require careful consideration for the mines experiencing large anisotropic deformation ground. The existing foliations impose a main challenge to control the rock mass bulking and shearing where bolts often becoming trapped and ‘guillotined’. To withstand the large displacement, appropriate surface support should be combined with bolts. Eftekhari and Aalianvari (2019) reported that the application of TBMs in great depth brings a significant change for engineers to overcome the problems in squeezing ground, some techniques were explained. However, it is hard to understand the failure mechanism and ground control in field. Therefore, numerical modeling has been widely utilized for designing underground openings. This method can simulate the different shapes of the excavation and various ground conditions such as complex geology structure, in-situ stress and mining-induced stresses conditions. Moreover, the numerical simulation tools also offer different support elements (i.e., cable, liner and beam, etc.) to study the influence of support system on the mechanical behavior of surrounding rock mass. Although the discrete element method is an appropriated tool to reflect the influence of joint structure, it is time-consuming and calculation-restriction (Sainsbury 2017). The continuum numerical simulation such as FLAC or FLAC3D is widely used to perform the large-scale modeling (Barla *et al.* 2011a). A ubiquitous-joint model is implemented to simulate the anisotropic behavior of rock mass (Itasca Consulting Group 2012) and was used by several authors (Watson *et al.* 2015, Vakili *et al.* 2014, Manh *et al.* 2015).

In this research, to realistically understand the rock mass anisotropic behavior in the macro-scale, the three-dimensional continuum numerical modeling was utilized. Moreover, the ubiquitous-joint model in FLAC3D was applied to describe the influence of foliation strike on the deformation and failure of the excavation. First, the model was verified based on the available monitoring data from the mine site. Subsequently, the influences of mining depth and intercept angle were studied and the relationships between mining depths, intercept angle and closure strain and damage region were presented. Finally, the presented support strategies were compared to optimize the ground support method. The influence of bolt spacing and ring spacing were also discussed.

2. Anisotropic large deformation in mine H

2.1 Geology condition of the deep hard rock mine site

A deep underground mine located in Western Australia is selected as a case study in this research. Mafic-ultramafic volcanics, felsic volcanoclastics and epiclastic sedimentary rocks generally exist in this mining domain. The width of the ore body is approximately 20 m with 80-90° dip and ~270° dip direction as shown in Fig. 2. There are no recorded major inflows of groundwater. The hanging wall and footwall mainly composite Basalt which is a typical hard rock with high intact rock strength. Basalt and Dolerite deposit in ore body (shear zone) where the foliation structure is obvious. Intense joint with 0.1-1 m spacing is measured in the shear zone. Although the hosted rock has high compressive strength, anisotropic deformation is significant and rock mass has low strength comparing to that in hanging wall and footwall. The current mining depth is nearly 700 m deep and it has been reported that exceptional potential is present to at least 1000 m. Moreover, the excavation axis is almost parallel to the strike of the ore body and also parallel with the strike of the foliation. As a result, the two side walls have large closure deformation. Table 1 lists the basic deformation and strength parameters of the rocks. The major principle stress (σ_1) is sub-horizontal and sub-perpendicular to the ore body which is 2-3 times of the vertical principle stress (σ_3). Table 2 lists the measured in-situ stress results. The horizontal stress is nearly 2.47 times of the vertical stress. Under high

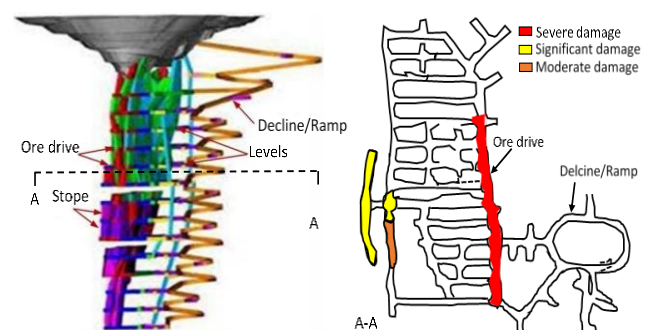


Fig. 2 Mining domains and damage zone in the case mine H

Table 1 Ranges of material properties of the intact rock and rock mass of mine H

Rock Type	σ_{ci} (MPa)	σ_t (MPa)	ρ (kg/m ³)	E (GPa)	ν	Q	GSI	σ_{cm} (MPa)	E_{rm} (GPa)	σ_{tm} (MPa)
Footwall/Hangingwall	190 ± 20	27 ± 4	2800	66 ± 7	0.15-0.29	5.4-26	60 ± 5	20.4 ± 6.6	34.5 ± 7.4	0.36 ± 0.16
Ore/Shear Zone	171 ± 14	16.7 ± 5	2600	48 ± 6	0.2-0.36	1.3-8.6	35 ± 5	4.1 ± 1.6	5.4 ± 2.3	0.061 ± 0.03

Table 2 Stress gradients at Mine H

In-situ stresses	Equation	Dip(°)	Dip direction (°)	Stress at depth H=700 m
Major stress σ_1	$0.075 \times H$	9-12	180-206	52.5 MPa
Intermediate stress σ_2	$0.0483 \times H$	14-19	97-115	33.81 MPa
Vertical stress σ_3	$0.0304 \times H$	67-73	307-329	21.28 MPa

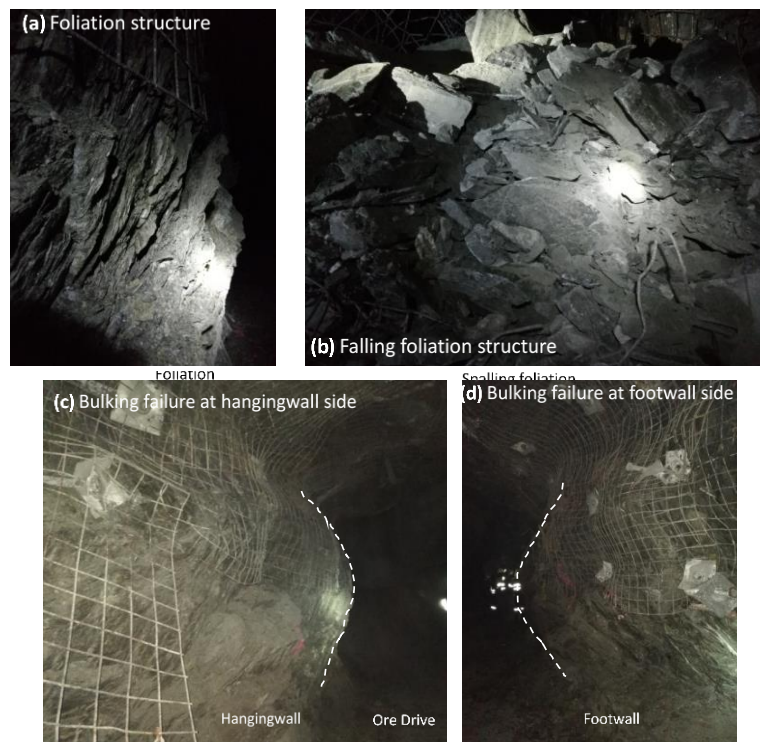


Fig. 3 Field observed foliation and bulking deformation of the two-side wall of ore drive

stress condition, the stress redistributes around the excavation and severe damage can be observed in field.

2.2 Anisotropic deformation and failure

As mentioned above, the horizontal stress is significantly larger than the vertical stress with a ratio of ~2.47. The direction of the maximum principal stress is nearly perpendicular to the strike of the shear zone which is also perpendicular to the excavation direction. This stress condition presents a potential large anisotropic deformation environment. Moreover, the intensive foliation induces to pronounced anisotropic failure of the opening. As shown in Fig. 3(a) and 3(b), obvious joint can be observed. Both the width and height of the ore drive is approximately 4 m. After excavation, stress redistributed and concentrated around the opening, the foliated rock mass deformed along the joint interface. Also, rock mass compressed in the

normal direction to the foliation which resulted in anisotropic deformation and failure as shown in Fig. 3(c) and 3(d). The two side walls bulked to the excavation space and the monitored closure deformation is larger than 80 cm.

3. Continuum numerical simulation of anisotropic deformation in FLAC3D

Both the continuum and discontinue methods are widely used to reproduce the mechanical behaviors of rocks. For simulating the anisotropic behavior of the jointed rock mass, the discrete element method (i.e., UDEC and 3DEC) is an appropriated tool. However, it is time consuming, computational restriction and low efficiency to simulate the large-scale geometry model although it can reflect the block rotation and the effect of joint spacing (Sainsbury and Sainsbury 2017, Yadav and Sharan 2019, Yao *et al.* 2019).

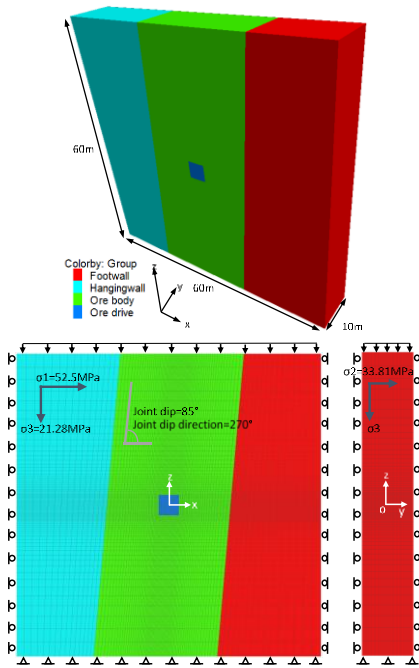


Fig. 4 3D numerical model of the case mine H

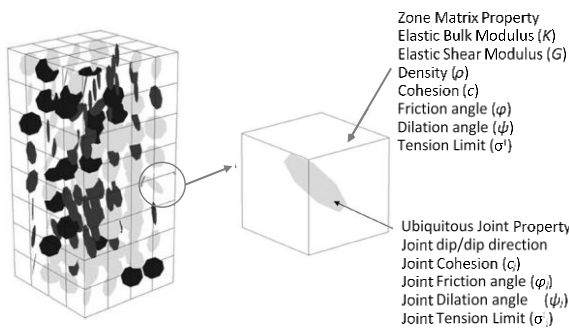


Fig. 5 Schematic diagram of the Ubiquitous-Joint model in FLAC3D (Modified after Sainsbury *et al.* 2017)

As a result, the continuum approach (i.e., FLAC and FLAC3D) is more popular for modeling the anisotropic behavior of the foliated ground using the improved model-ubiquitous-joint model (Itasca Consulting Group 2012). This model can describe the influence of joint dip and orientation on the mechanical behavior of the foliated rock mass. Therefore, this work utilized the ubiquitous-joint model to reproduce the anisotropic deformation of the surrounding rock in large anisotropic deformation ground.

3.1 Model construction

In this research, three-dimensional numerical model was first built in FLAC3D program. The geometry of the researched mine model is $60 \text{ m} \times 10 \text{ m} \times 60 \text{ m}$. The shape of the ore drive was approximately set as rectangle with $4 \times 4 \text{ m}$ size. Based on the geological information, the width of the ore body is set as 20 m. The minimum size of the element zone around the excavation is set as 0.2 m which satisfies the calculation efficiency and accuracy. For boundary conditions, the velocities in X, Y and Z directions are restricted at the bottom of the geometry boundary. The

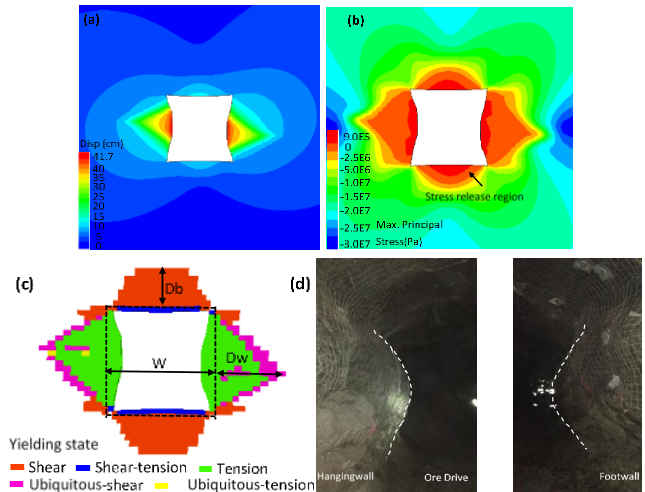


Fig. 6 Modelling deformation, the Max. principal stress distribution and yielding state

velocities in the normal direction of the side faces are fixed. A normal vertical stress is applied on the top face of the model. The in-situ stress σ_1 , σ_2 and σ_3 at 700 m depth is 52.5, 33.81 and 21.28 MPa, respectively. The details of the boundary conditions of the model is presented in Fig. 4.

3.2 Anisotropic constitutive model

In FLAC3D, the ubiquitous-joint model is developed to describe the influence of weakness plane on the mechanical behavior of material showing anisotropic characteristic. In this model, the orientation of the weakness can be considered in finite difference zone. The model parameters can be classified as two kinds, including zone matrix property and ubiquitous-joint property as presented in Fig. 5. This model does not consider the joint spacing or size of the weakness plane. The strength criteria used in the zone matrix and along the weakness is Mohr-Coulomb envelop with a tension cut-off (Itasca Consulting Group 2012).

The failure mechanism of the rock mass around the underground openings in jointed ground is dependent on the relative angle between excavation and orientation of the foliation. To put reasonable support strategies and manage the excavation deformation, the failure mechanisms should be first understood. Therefore, the large anisotropic deformation and failure mechanism of the ore drive observed in mine H is simulated by FLAC3D using the ubiquitous-joint model.

3.3 Model calibration

Table 1 presents the basic rock mechanical parameters. But they cannot be directly used in simulation. The intact rocks have good integrity and high strength which does not consider the orientation of the joint. In the ubiquitous-joint model, the parameters of the zone matrix and weakness plane should be calibrated. Based on the monitored deformation of the ore drive, the parameters were first calibrated using back-analysis method.

First, the elastic model was assigned to the whole model

Table 3 Calibrated numerical calculation parameters of the ubiquitous-joint model

Zone matrix property							
Rock Type	ρ (kg/m ³)	E (GPa)	ν	φ (°)	c (MPa)	ψ (°)	σ_1 (MPa)
Footwall Hangingwall	2800	3.7	0.25	41.5	14.1	10	1.41
Ore/Shear Zone	2600	1.8	0.3	36	9.5	9	0.95
Foliation property							
Joint dip (°)	Joint DD (°)	c_j (MPa)	σ_{ij} (MPa)	φ_j (°)	ψ_j (°)		
85	270	0.3	0.03	35	9		

to calculate the initial equilibrium. This aim is to avoid the model yielding before excavation. After obtained the initial equilibrium model under the applied initial in-situ stress, the model displacement, velocity and state were initialized. Subsequently, the ubiquitous-joint constitutive model was used in the model. A series of numerical calculation and iterations were performed to calibrate the numerical calculation parameters. Table 3 presents the material parameters used in the model which are calibrated according to the field recorded deformation of the ore drive after excavation.

In Fig. 6(a), the maximum wall deformation in simulation reaches to 41.7 cm which goes well with the measured data in field. Singh *et al.* (2007) suggested that the critical strain can be used to evaluate the squeezing condition. The wall closure strain (ε) can be calculated by Eq. (1). As a result, the wall closure strain reaches to 20.9% showing large closure deformation. After excavation, stress redistributed around the opening, the maximum principal stress can describe the stress state at near the mining ore drive. Fig. 6(b) provides the distribution of the maximum principal stress. The stress around the excavation boundary is mainly composed of tension force about 0.9 MPa. Shear failure occurred in deep zones whereas tensile failure occurred near the excavation face which induces dilation and large convergence. The stress near 0 MPa can be regarded as a stress release boundary. From the excavation sides to the stress release region, the previous high stress concentration induced zone or weakness plane to yield and new stress concentration gradually moved to the far field. The size of the stress release region can indirectly denote the tension damage degree of the surround rocks. It is clear that the stress release region in two side wall directions are larger than that in back-floor direction. This indicates that the foliation parallel to the excavation direction occurs much severe damage. Moreover, the zone and weakness yielding state are also plotted in Fig. 6(c). The yielding region in two side wall direction (model x direction) is larger than that in back and floor direction (model z direction). This results also suggests that the orientation of joint exerts significant influence on the failure extent of the excavation.

$$\text{Closure strain}(\varepsilon) = \frac{\text{Original width} - \text{Current width}}{\text{Original width}} \times 100\% \quad (1)$$

4. Critical factors influencing the anisotropic deformation of excavation

In-situ stress and the relative location of the excavation and foliation significantly influence the mechanical behavior of foliated rock mass. High stress induces severe stress concentration and failure. The deformation response and failure mechanism are controlled by the foliation orientation. Therefore, these two crucial factors are investigated in this section to explore the quantitative relations of deformation and failure mechanism in the case mine H.

4.1 Influence of intercept angle

The relative angle of the foliation orientation and excavation direction can be described by the intercept angle (ω) as illustrated in Fig. 7. In foliated underground mining, it is inevitable that the mining ore drives will pass through the jointed rock mass. Therefore, a favorable intercept angle can reduce the deformation and damage state around the openings. Schubert and Mendez (2017) pointed that the deformation varies by order of magnitude as relative orientation changes from perpendicular to parallel direction. The deformation has a nonlinear relation with intercept angle between foliation strike and excavation axis (Karampinos and Hadjigeorgiou *et al.* 2017, Yadav and Sharan 2019). To better understand the influence of intercept angle on the closure deformation of ore drive in mine H and obtain the quantitative relation, seven intercept angles (varying from 0 to 90°) are compared in the calibrated model. The joint dip keeps constant as 85° and the dip direction of the joint is changed according to the expected set values in the ubiquitous-joint model.

It should be noted that the calculation needs long time, so the 3D models with 1m thickness in Y direction were used to simplify the analysis of the influence of mining depth and foliation orientation. Fig. 8 compares the simulation results of the displacement, the maximum principal stress and yielding state of the model considering the influence of different intercept angles. As the intercept angle (ω) increases from 0 to 90°, the stress release region in back-floor direction (axial z direction) has no obvious change, whereas that in two-side wall direction (axial x direction) decreases significantly. The magnitude of the displacement and the yielding region also decrease gradually with increasing intercept angle. This suggests that the orientation of the foliation has significant influence on the deformation and failure of the excavation.

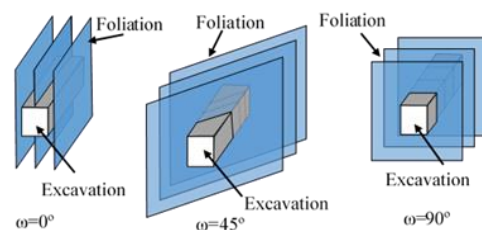


Fig. 7 Intercept angle between excavation axis and foliation strike

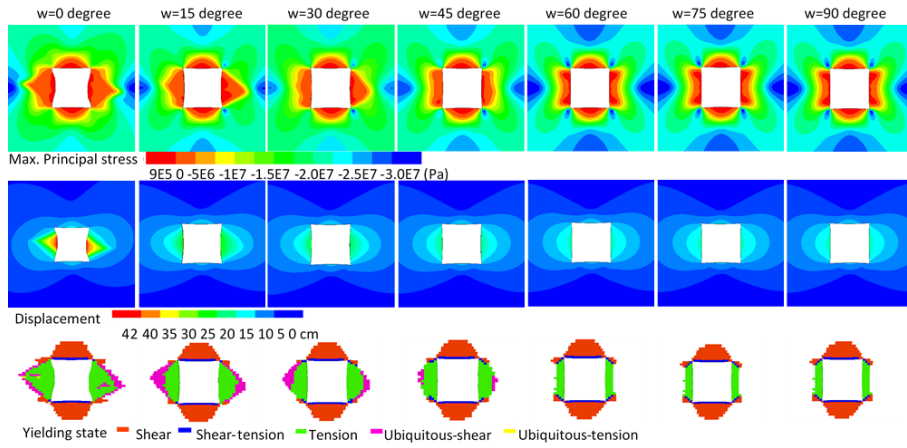


Fig. 8 The distribution characteristics of the maximum principal stress (upper figures), displacement (middle figures) and yielding state (lower figures) with different intercept angles

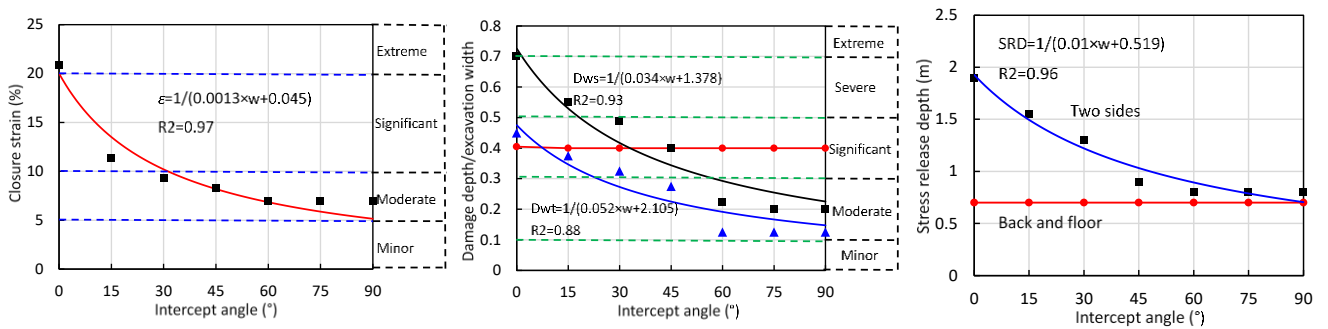


Fig. 9 Relationships between intercept angle and closure strain, damage depth/excavation width and stress release depth

Table 4 Monitored results of the numerical simulation models with different intercept angles

Intercept angle-w (°)	0	15	30	45	60	75	90
Deformation (cm)	41.8	22.73	18.7	16.6	14.0	13.98	13.97
Damage ratio-(Dws/W)	0.70	0.55	0.49	0.40	0.22	0.20	0.20
Damage ratio-(Dwt/W)	0.45	0.38	0.33	0.28	0.13	0.13	0.13
Damage ratio-(Db/W)	0.40	0.40	0.40	0.40	0.40	0.40	0.40
Stress release-back-floor (m)	0.7	0.7	0.7	0.7	0.7	0.7	0.7
Stress release-hanging-footwall (m)	1.9	1.55	1.3	0.9	0.8	0.8	0.8

Note: Dws: shear damage depth at hanging-footwall side; Dwt: tensile damage depth at hanging-footwall side; Db: damage depth at back-floor side; W: excavation width

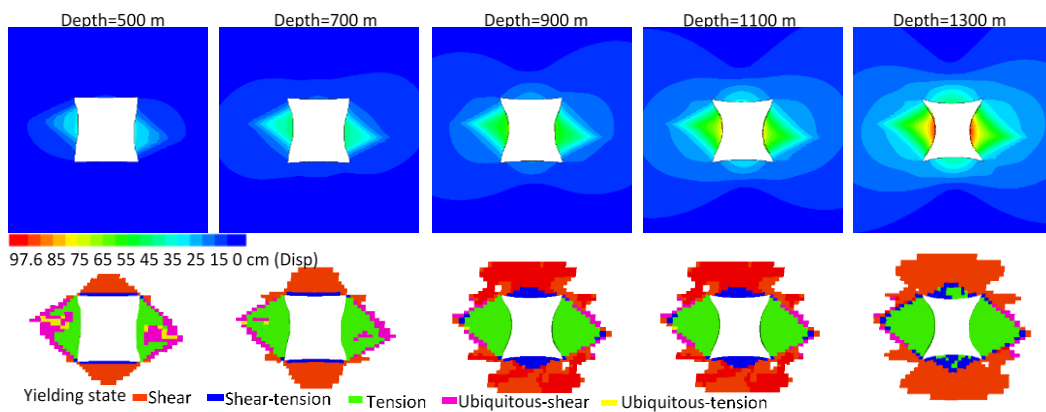


Fig. 10 Displacement and yielding state of the model at different mining depths

Table 5 Monitored results of the numerical simulation models with different mining depth

Mining depth (m)	500	700	900	1100	1300
Displacement (cm)	27.4	41.8	63.2	79.7	97.7
Closure strain (%)	13.3	22	34.63	58	88
Damage ratio-back and floor	1.7	1.75	1.88	1.88	2.68
Damage ratio- hanging-footwall	0.58	0.78	1.03	1.18	1.5

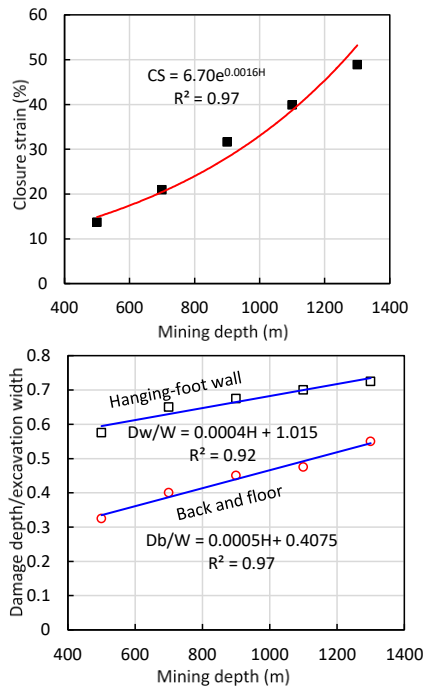


Fig. 11 Relationships between mining depth and closure strain and damage depth/excavation width

To investigate the quantitative relations between the monitored values and intercept angle, Table 4 collects the details of the simulations based on Fig. 8. In Fig. 9, the detailed relations are presented. The closure strain, the damage depth/excavation width and the stress release width in hanging-footwall side direction have nonlinear correlations with increasing intercept angle. However, the intercept angle has little influence on the variations in back-floor direction. These quantitative relations can provide a reference for predicting the deformation and damage degree in foliated underground excavation. Furthermore, the damage induced by excavation can be characterized as different levels according to the closure strain or the damage depth/excavation width. It should be noted that the intercept angle has no obvious influence on the closure deformation and damage at the back-floor direction, therefore, the influence at the two-side wall direction is investigated to explore the anisotropic characteristics.

4.2 Influence of excavation depth

In addition, the mining depth also has a significant effect on the deformation and failure of the excavation. To investigate the deformation and failure extent of the

excavations at different mining depths, this simulation performed five mining depths modeling cases. Fig. 10 plots the displacement and yielding state of the model at different mining depths. As the mining depth increases from 500 m to 1300 m, the closure deformation increases from 27.4 cm to 97.7 cm and the yielding region around the excavation gradually increases. This suggests that the large deformation and failure will become much severe in increasing mining depth. Table 5 lists the details of the information in Fig. 10. Fig. 11 presents the quantitative relationships between mining depth and closure strain and damage depth/excavation depth showing significant nonlinear correlations. This results also provide a reference for predicting the deformation and damage of the opening under deep mining.

5. Support system performance for managing large anisotropic deformation

Ground support systems are selected according to the field condition. Based on the modeling results, the ratios of the shear and tension damage depth to the excavation width is nearly 0.7 and 0.45, respectively. Therefore, the length of the rockbolt is selected as 2.4 m and diameter of 20 mm. To reduce the influence of probable seismicity and increase the energy absorption capacity of reinforcement system, the resin anchored length at two ends of the rockbolt is set as 0.6 m and 1.4 m in middle left without encapsulation. Moreover, the foliation structure reduces the integrity of the surrounding rock, so the cable with 6.5 m length and diameter of 15.2 mm with 6 m encapsulation length is used to fix with the far away undamaged rock. In addition, some surface support such as the combinations of shotcrete, mesh split sets are utilized in the deep underground with high stress condition (Barla *et al.* 2011b, Stephenson and Sandy 2017). Therefore, composite of shotcrete and mesh elements is used in mine H. The combination of the surface support can obtain a much efficient controlling effect. So, four cases will be compared in the following analysis with 10 m thickness models in Y axis.

5.1 Reinforcement by the cables and rockbolts

The layout of the reinforcement by cable and rockbolt is detailed in Fig. 12 where the support patterns in back view and two-side wall view of the ore drive are plotted. The ring spacing in the excavation direction is set as 1m and the bolt spacing is also set as 1m. It should be noted that in the excavation direction, the support pattern is different showing interaction by rockbolt and cable as shown in A-A and B-B cut planes. The black line represents the cable bolt and the red and blue line represents the rockbolt whose free section is shown by the blue line and the fixed section is noted by red lines. Table 6 lists the parameters of the bolts in simulation.

5.2 Surface support by a composite of shotcrete and mesh

An important method to control the ongoing

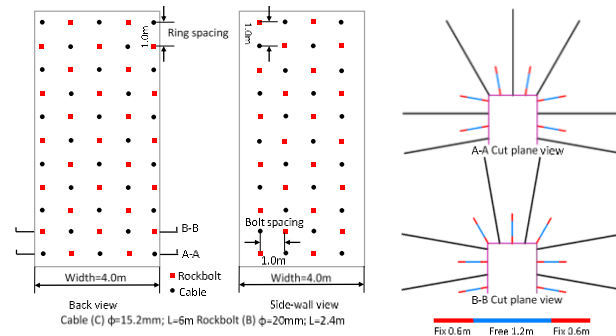


Fig. 12 Layout of the reinforcement applied in the ore drive

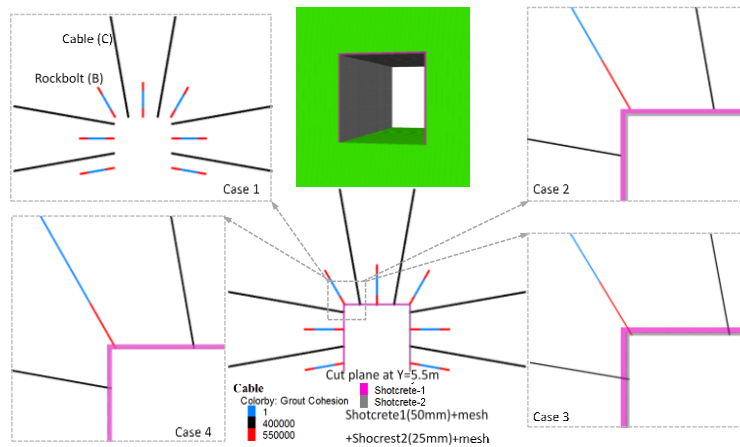


Fig. 13 Details of the different support patterns in the simulation Note: Case 1: Install Reinforcement (cablebolts and rockbolts) only, Case 2: First install reinforcement (cablebolts and rockbolts) and then install surface support (two layers of shotcrete and mesh), Case 3: First install surface support (two layers of shotcrete and mesh) and then install reinforcement (cablebolts and rockbolts), Case 4: First install reinforcement (cablebolts and rockbolts) and then install surface support (one layer of shotcrete and mesh)

Table 6 Parameters of the rockbolt and cable in this simulation

	Grouted type	Length (m)	Diameter (mm)	Area (m ²)	E (GPa)	Tensile limit (kN)	Bond stiffness (N/m/m)	Cohesive of bond (N/m)
Rockbolt	two-ends grouted	2.4	20	3.14E-4	200	185	1.5E7	550E3
Cable	Fully grouted	6.0	15.6	1.99E-4	200	261	5.56E6	400E3

Table 7 Installation details in the modeling cases

Cases	First installation step	Second installation step
Case1	Rockbolt ($\varphi=20$ cm $L=2.4$ m) both ends anchored	No
Case2	Cablebolt ($\varphi=15.6$ cm $L=6.0$ m) Fully grouted	layer1: Shotcrete+mesh (50 mm)
Case3	Rockbolt ($\varphi=20$ cm $L=2.4$ m) both ends anchored	layer2: Shotcrete +mesh (25 mm)
Case4	Cablebolt ($\varphi=15.6$ cm $L=6.0$ m) Fully grouted	Rockbolt ($\varphi=20$ cm $L=2.4$ m) both ends anchored

Table 8 Parameters of the steel fibre reinforced shotcrete from Saw *et al.* (2013) and simulation simplification

	Density(kg/m ³)	Young's modulus (GPa)	Poisson's ratio	Cohesion (MPa)	Frictional angle (°)	Tensile strength (MPa)
Lab test	2344-2357	14-16	0.17-0.22	5-8	35-40	3.6-4.4
Simulation	2350	15	0.2	-	-	-

Note: Elastic model was used to simulate the combination of the shotcrete and mesh

deformation is the utilization of the fibrecrete and weld

mesh. The fibrecrete can provide an early confinement to

control the excessive failure of the surrounding rock moving to the excavation space. The mesh can prevent the large-area cracking. Therefore, the surface support is also applied in mine H to reduce the effect of the large anisotropic deformation failure of the excavation. To compare the controlling effect of the different support patterns, four cases are compared in the simulation. For the case 1, it does not consider the surface support. The support element composites of resin rockbolt and cable as shown in Fig. 13 and the reinforcement layout is presented in Fig. 13. For the case 2, the same reinforcement is applied whereas adding two layers shotcrete and mesh. After installing the rockbolts and cables, the first layer shotcrete with 50 mm thickness is added to the surface of the excavation, subsequently, another layer shotcrete with 25 mm thickness is continually performed. For the case 3, in order to compare the influence of installation sequence, the same support elements are utilized but using an inverse installation sequence. This means that the surface support is first installed and then install the reinforcement. For the case 4, the reinforcement is first installed and then just one-layer shotcrete with 50 mm thickness is added. Table 7 presents the parameters of the shotcrete. It should be noted that elastic constitutive model is used to simulate the composite of the shotcrete and mesh. Table 7 lists the details of the support cases.

6. Numerical simulation of the support system installation scenarios

Case 1 Install Reinforcement (cablebolts and rockbolts) only

In this case, the influence of the reinforcement is just analyzed. To describe the two-ends resin anchored effect of the rockbolt and to simulate the tray, the anchored-end of rockbolt at the excavation space side is simulated by the rigid contact between the near zone and the end-node of the cable element. Moreover, a pre-tension force with 100 kN is applied on the cable and rockbolt to increase our understanding of this simulation effect. Fig. 14 presents the anchored effect of the two-ends anchored rockbolt and fully grouted cable. It shows that the stray can be simulated and the reinforcement can increase the confinement of the surrounding rock mass.

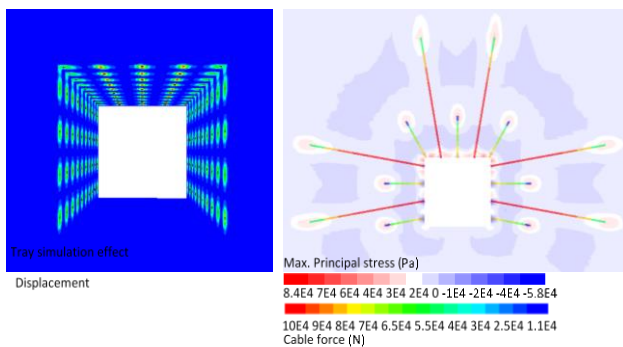


Fig. 14 Simulation results of the two-ends anchored rockbolts and fully grouted cable under 100 kN pre-tension force

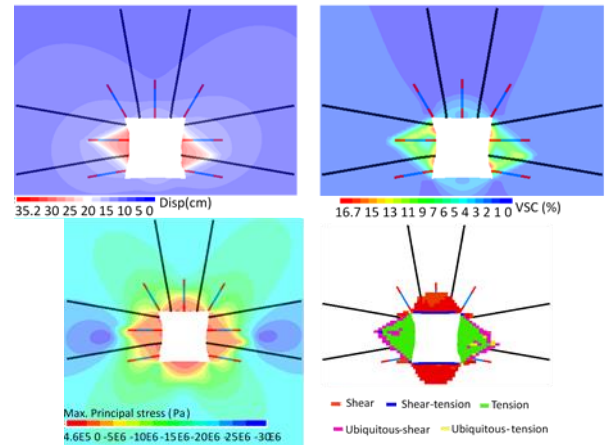


Fig. 15 The displacement, volumetric strain increment, max.principal stress and yielding state of the model in case 1

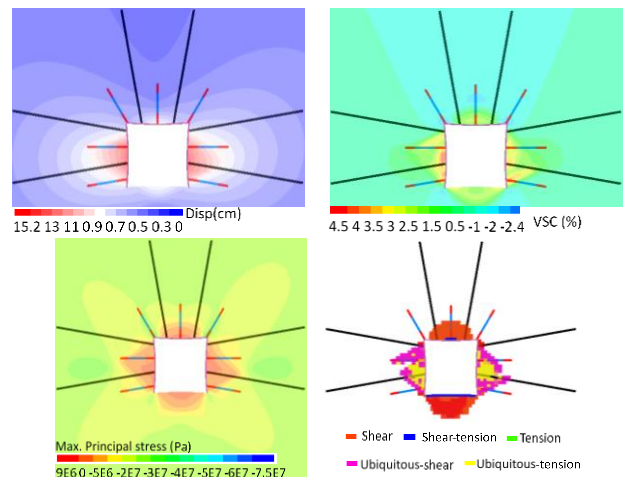


Fig. 16 The displacement, volumetric strain increment, max. principal stress and yielding state of the model in case 2

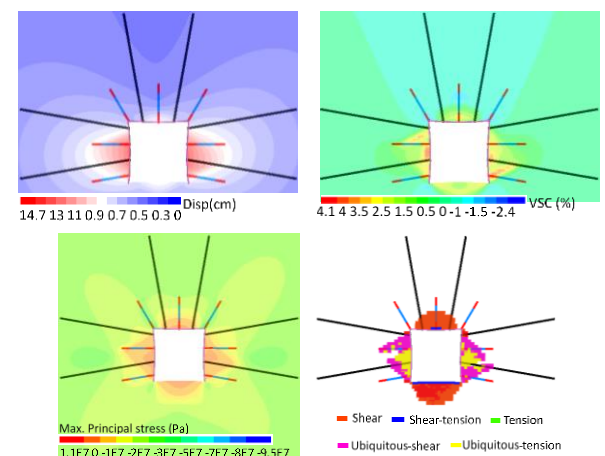


Fig. 17 The displacement, volumetric strain increment, max.principal stress and yielding state of the model in case 3

Fig. 15 presents the simulation results of the case 1 where the maximum displacement and volumetric strain

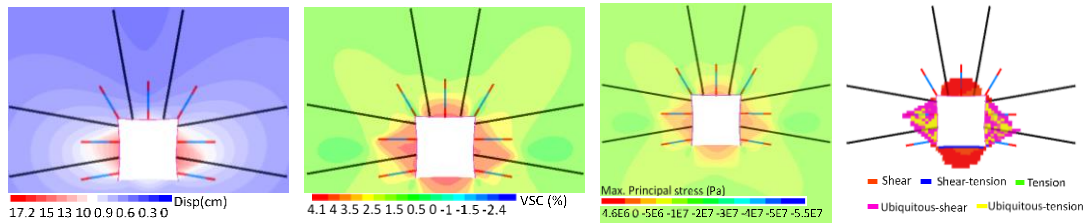


Fig. 18 The displacement, volumetric strain increment, max.principal stress and yielding state of the model in case 4

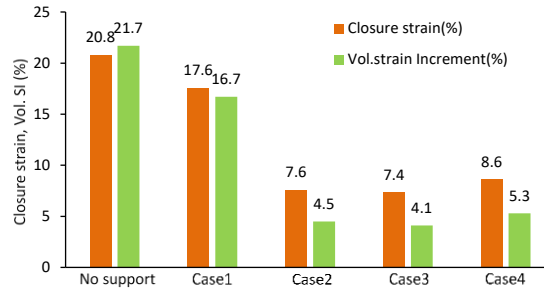


Fig. 19 Comparison with the closure strain and volumetric strain increment results in different support conditions

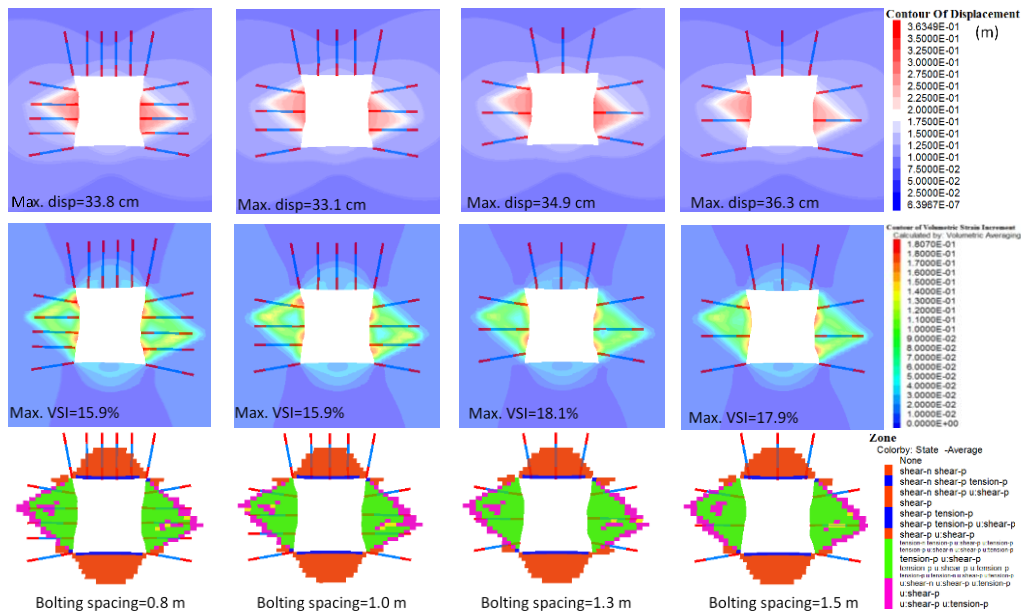


Fig. 20 Influence of bolting spacing on the displacement, vol. strain increment and yielding state

Table 9 Results of the case studies in this research

	Displacement (cm)	Closure strain (%)	Vol. strain Increment (%)	Max. principal stress (Pa)
No support	41.8	20.8	21.7	8.8E5
Case 1	35.1	17.6	16.7	4.6E5
Case 2	15.2	7.6	4.5	9.0E6
Case 3	14.7	7.4	4.1	1.14E7
Case 4	17.2	8.6	5.3	4.6E6

increment reach to 35.2 cm and 16.7%, respectively. Due to the influence of the foliation, large deformation occurs mainly at the two-side walls. The counter of the maximum principal stress denotes that the stress release region at the two-side walls is larger than that at the back-floor side. The

yielding state around the excavation also denotes that the tension failure mainly occurred at the two walls and shear failure occurs mainly at the back and floor.

Case 2 First install reinforcement (cablebolts and rockbolts) and then install surface support (two layers of shotcrete and mesh)

In this case, surface support elements are added except for the reinforcement elements. Similar to the case 1, the rockbolts and cables are first installed. Subsequently, one-layer shotcrete+mesh with 50 mm and another layer shotcrete+mesh with 25 mm are installed one by one. The modeling results are summarized in Fig. 16. Compare to the results obtained in case 1, the maximum displacement and volumetric strain reduce to 15.2 cm and 4.5%, respectively.

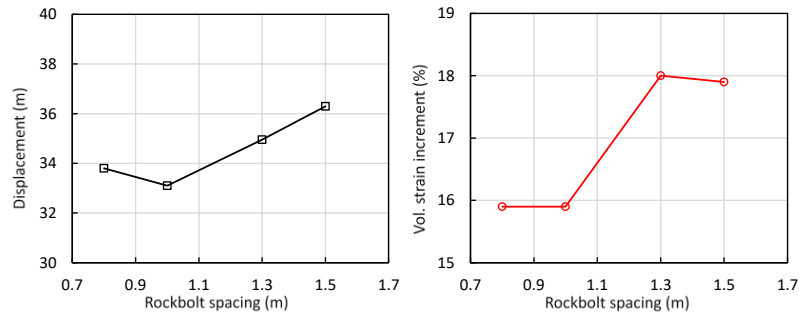


Fig. 21 Relationships between rockbolt spacing and displacement and vol. strain increment

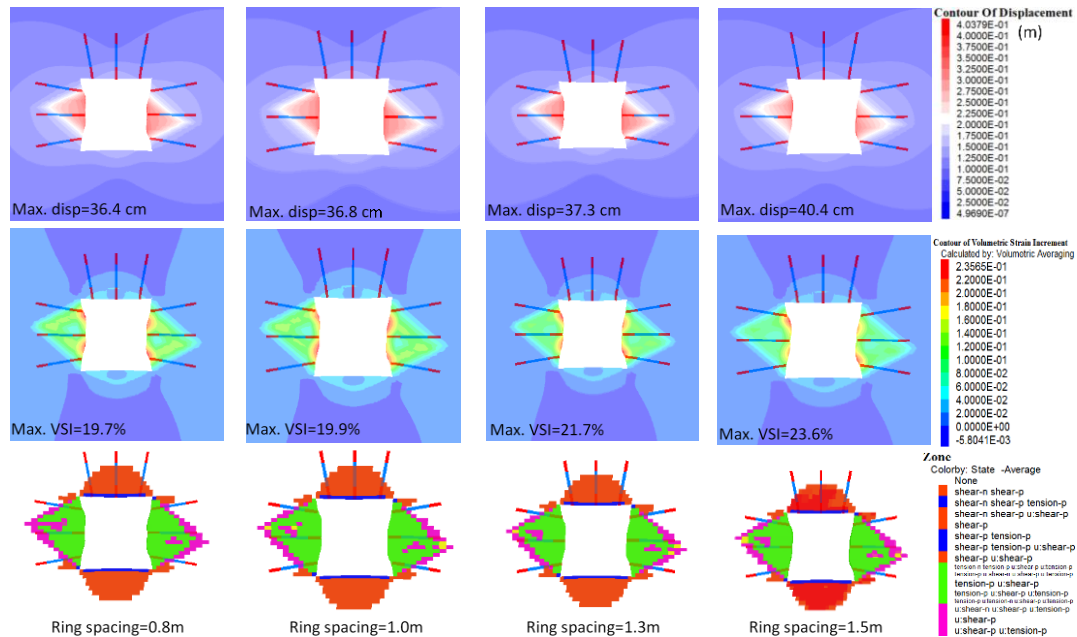


Fig. 22 Influence of ring spacing on the displacement, vol. strain increment and yielding state

The tension failure region has a significant reduction when applied the surface support. This suggests that the surface support technology has good effect for controlling the large deformation and tensile failure can be constrained effectively.

Case 3 First install surface support (two layers of shotcrete and mesh) and then install reinforcement (cablebolts and rockbolts)

To compare the effect of the installation sequence on the deformation and damage degree of the excavation, this case first installs shotcrete+mesh and then install rockbolts and cables. The modeling results are illustrated in Fig. 17 where the maximum deformation and volumetric strain increment is 14.7 cm and 4.1%, respectively, which are smaller than those in the case 3 results. This suggests that first install the surface support will enhance the integrity of the rock mass and reduce the closure deformation. The increase in the maximum principal stress means that the composite support can provide a larger confinement to the damaged rock mass near the excavation space. The yielding region of the zone has no significant change.

Case 4 First install reinforcement (cablebolts and rockbolts) and then install surface support (one layer of shotcrete and mesh)

Moreover, the case 4 investigates the effect of the shotcrete layer on the displacement and failure of the ore drive. One-layer shotcrete with 50 mm thickness and one-layer mesh were first implemented and then install the cables and rockbolts. As presented in Fig. 18, the maximum closure deformation and the volumetric strain increment is 17.2 cm and 4.1%, respectively. The yielding region around the excavation seems little larger than that in sidewall comparing to that in case 3. This case denotes that the effect of using a layer of concrete is worse than that of the two layers.

The detail results of the case studies are tableted in Table 9. Fig. 19 presents the closure strain and volumetric strain increment results of the excavation under different support increment patterns. Both the closure strain and volumetric strain increment show larger values (i.e., 20.8% and 21.7%, respectively) than those under support conditions. In case 3, those values are the lowest (i.e., 7.4% and 4.1%, respectively) which suggests that first install two layers

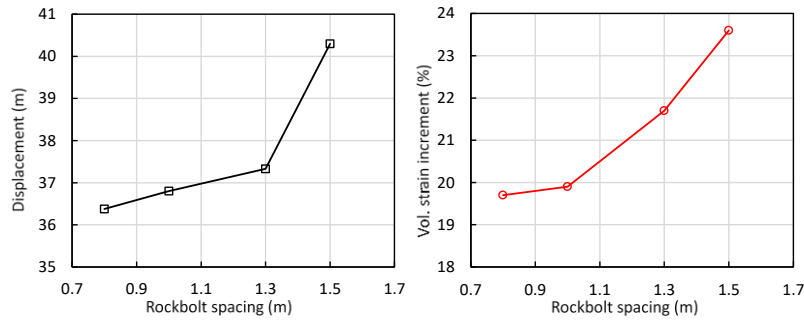


Fig. 23 Relationships between ring spacing and displacement and vol. strain increment

Table 10 Results of the deformation of the excavation with different support patterns

Rockbolt spacing	Displacement (cm)	Closure strain (%)	Vol. strain Increment (%)
0.8	33.8	16.9	15.9
1.0	33.1	16.6	15.9
1.3	34.9	17.5	18.0
1.5	36.3	18.2	17.9
Ring spacing	Displacement (cm)	Closure strain (%)	Vol. strain Increment (%)
0.8	36.4	18.2	19.7
1.0	36.8	18.4	19.9
1.3	37.3	18.7	21.7
1.5	40.3	20.2	23.6

shotcretes and then install reinforcement will obtain a better effect for controlling the large anisotropic deformation of the excavation.

7. Discussion on different support patterns

Except for the influence of reinforcement and surface support and its installation sequence, the reinforcement installation spacing also has a great influence on the displacement magnitude. The installation spacing can be divided into two kinds of spacing including rockbolt spacing and ring spacing. This section will discuss these two influencing factors.

7.1 Influence of rockbolt spacing

At a same cut plane section, different bolts installation spacing will produce various controlling effects. Installing dense anchors will increase support costs but installing loose bolts cannot effectively control the surrounding rock mass. Therefore, here uses four rockbolts spacing values (i.e., 0.8, 1.0, 1.3 and 1.5 m) to compare the controlling effects. Figs. 20 and 21 present the comparing results of the different bolt spacing cases. The displacement increases gradually as the rockbolt spacing increases as well as the volumetric strain increment. However, the rockbolt installation spacing has no obvious influence on the yielding state region. The high-stress environment can induce different cross-section closure magnitudes in Table 10.

7.2 Influence of rockbolt ring spacing

If the rockbolt installation spacing at a same cut plane section is kept unchanged, just adjust the ring spacing along the excavation direction. This will produce different results. Keeping the rockbolt spacing as 1.3 m at each section, the ring spacing varies from 0.8 to 1.5 m. The displacement, volumetric strain increment and yielding state are presented in Fig. 22. Fig. 23 summarizes the relationships between ring spacing and displacement and volumetric strain increment. It suggests that larger ring spacing will reduce the controlling effect showing relatively large deformation volumetric increment. The details are also listed in Table 10.

8. Conclusions

This research performed case study and numerical simulation to investigate the large anisotropic behavior of the ore drive excavated in large anisotropic deformation ground located in Western Australia. To investigate the influence of foliation orientation, the ubiquitous-joint model was used in FLAC3D. Numerical simulation was calibrated to reproduce the observed anisotropy of the two sidewalls of the ore drive. Based on the verified model, the roles of mining depth and intercept angle affecting on the anisotropy were researched. Subsequently, the composite support technology was utilized and compared to obtain an effective controlling effect. The influence of bolt spacing and ring spacing were also discussed. The outcomes are listed as follows:

- Anisotropic large deformation was induced by the squeezing condition with high-stress and foliation ground. The numerical modeling using the ubiquitous-joint model agrees well with the observed phenomena in the mine site.
- The wall-to-wall closure strain, damage depth and stress release region decreased nonlinearly with increasing intercept angle, whereas they increased as mining depth increases. Damage levels can be classified by the closure strain and damage depth where the closure strain and shear damage depth/excavation width decrease from 20.9% to 7.0% and 0.7 to 0.2, respectively.
- The comparison of the composite support strategies show that the surface support can significantly reduce the

tension failure extent at the two side walls near the excavation space. First install surface support and then install reinforcement can obtain a good effect for controlling the large deformation of the ore drive.

- Comparing the controlling effect by different bolt spacing and ring spacing, an appropriate spacing can be selected based on the field condition and support cost. The outcomes obtained in this research may serve to enhance mining engineer's confidence in controlling the ore drive stability excavated in foliated ground.

Acknowledgments

This work is financially supported by the National Natural Science Foundation of China (No. 51874175; No. 51974145), the Project of Young Talents in Science and Technology of the Department of Education of Liaoning Province (LJ2019QL005), Key Scientific Research Project of Inner Mongolia Universities (NJZZ20300), and National Natural Science Foundation of China the 111 Project under grant no: 51839003 and B17009.

References

- Aksoy, C.O., Aksoy, G.G.U., Guney, A., Ozacar, V. and Yaman, H.E. (2020), "Influence of time-dependency on elastic rock properties under constant load and its effect on tunnel stability", *Geomech. Eng.*, **20**(1), 1-7. <https://doi.org/10.12989/gae.2020.20.1.001>.
- Bagheripour, M.H., Rahgozar, R., Pashnesaz, H. and Malekinejad, M. (2011), "A complement to Hoek-Brown failure criterion for strength prediction in anisotropic rock", *Geomech. Eng.*, **3**(1), 61-81. <https://doi.org/10.12989/gae.2011.3.1.061>.
- Barla, G., Bonini, M. and Semeraro, M. (2011b), "Analysis of the behaviour of a yield-control support system in squeezing rock", *Tunn. Undergr. Sp. Technol.*, **26**(1), 146-154. <https://doi.org/10.1016/j.tust.2010.08.001>.
- Barla, G., Debernardi, D. and Sterpi, D. (2011a), "Time-dependent modeling of tunnels in squeezing conditions", *Int. J. Geomech.*, **12**(6), 697-710. [https://doi.org/10.1061/\(ASCE\)GM.1943-5622.0000163](https://doi.org/10.1061/(ASCE)GM.1943-5622.0000163).
- Eftekhari, A. and Aalianvari, A. (2019), "An overview of several techniques employed to overcome squeezing in mechanized tunnels; A case study", *Geomech. Eng.*, **18**(2), 215-224. <https://doi.org/10.12989/gae.2019.18.2.215>.
- Itasca Consulting Group Inc. (2012), *FLAC3D—Fast Lagrangian Analysis of Continua (Version 5.0)*, Itasca, Minneapolis, Minnesota, U.S.A.
- Karampinos, E. and Hadjigeorgiou, J. (2017), "Quantifying the influence of structure, rock mass strength and mining development of drives in squeezing ground", *Min. Technol.*, **127**(4), 177-194. <https://doi.org/10.1080/14749009.2017.1409983>.
- Kazakidis, V.N. (2002), "Confinement effects and energy balance analyses for buckling failure under eccentric loading conditions", *Rock Mech. Rock Eng.*, **35**(2), 115-126. <https://doi.org/10.1007/s006030200015>.
- Kolymbas, D., Fellin, W. and Kirsch, A. (2006), "Squeezing due to stress relaxation in foliated rock", *Int. J. Numer. Anal. Meth. Geomech.*, **30**(13), 1357-1367. <https://doi.org/10.1002/nag.530>.
- Manh, H.T., Sulem, J., Subrin, D. and Billiaux, D. (2015), "Anisotropic time-dependent modeling of tunnel excavation in squeezing ground", *Rock Mech. Rock Eng.*, **48**(6), 2301-2317. <https://doi.org/10.1007/s00603-015-0717-y>.
- Meguid, M.A. and Rowe, R.K. (2006), "Stability of D-shaped tunnels in a Mohr-Coulomb material under anisotropic stress conditions", *Can. Geotech. J.*, **43**(3), 273-281. <https://doi.org/10.1139/T06-004>.
- Sainsbury, B.L. and Sainsbury, D.P. (2017), "Practical use of the ubiquitous-joint constitutive model for the simulation of anisotropic rock masses", *Rock Mech. Rock Eng.*, **50**(6), 1507-1528. <https://doi.org/10.1007/s00603-017-1177-3>.
- Sandy, M., Sharrock, G., Albrecht, J. and Vakili, A. (2010), "Managing the transition from low-stress to high-stress conditions", *Proceedings of the 2nd Australasian Ground Control in Mining Conference*, Sydney, Australia, November.
- Sandy, M.P., Gibson, W. and Gaudreau, D. (2007), "Canadian and Australian ground support practices in high deformation environments", *Proceedings of the 4th International Seminar on Deep and High Stress Mining*, Perth, Australia, November.
- Saw, H., Villaescusa, E., Windsor, C.R. and Thompson, A.G. (2013), "Laboratory testing of steel fibre reinforced shotcrete", *Int. J. Rock Mech. Min. Sci.*, **57**, 167-171. <https://doi.org/10.1016/j.ijrmm.2012.08.008>.
- Schubert, W. and Mendez, J.M.D. (2017), "Influence of foliation orientation on tunnel behavior", *Procedia Eng.*, **191**, 880-885. <https://doi.org/10.1016/j.proeng.2017.05.257>.
- Singh, M., Singh, B. and Choudhari, J. (2007), "Critical strain and squeezing of rock mass in tunnels", *Tunn. Undergr. Sp. Technol.*, **22**, 343-350. <https://doi.org/10.1016/j.tust.2006.06.005>.
- Stephenson, R.M. and Sandy, M.P. (2017), "Ground control methods in squeezing and rockburst-prone ground in mining—case studies and benchmarking", *Proceedings of the 8th International Conference on Deep and High Stress Mining*, Perth, Australia, March.
- Vakili, A., Albrecht, J. and Sandy, M. (2014), "Rock strength anisotropy and its importance in underground geotechnical design", *Proceedings of the AusRock 2014, 2nd Australasian Ground Control in Mining Conference*, New South Wales, Australia, November.
- Vu, T.M., Sulem, J., Subrin, D., Monin, N. and Lascols, J. (2013), "Anisotropic closure in squeezing rocks: The example of Saint-Martin-la-Porte access gallery", *Rock Mech. Rock Eng.*, **46**(2), 231-246. <https://doi.org/10.1007/s00603-012-0320-4>.
- Watson, J.M., Vakili, A. and Jakubowski, M. (2015), "Rock strength anisotropy in high stress conditions: A case study for application to shaft stability assessments", *Studia Geotechnica et Mechanica*, **37**(1), 115-125. <https://doi.org/10.1515/sgem-2015-0013>.
- Wu, K. and Shao, Z.S. (2019a), "Visco-elastic analysis on the effect of flexible layer on mechanical behavior of tunnels", *Int. J. Appl. Mech.*, **11**(3), 1950027. <https://doi.org/10.1142/S1758825119500273>.
- Wu, K. and Shao, Z.S. (2019b), "Study on the effect of flexible layer on support structures of tunnel excavated in viscoelastic rocks", *J. Eng. Mech.*, **145**(10), 04019077. [https://doi.org/10.1061/\(ASCE\)EM.1943-7889.0001657](https://doi.org/10.1061/(ASCE)EM.1943-7889.0001657).
- Wu, K., Shao, Z.S., Qin, S. and Li, B.X. (2020), "Determination of deformation mechanism and countermeasures in silty clay tunnel", *J. Perform. Construct. Facil.*, **34**(1), 04019095. [https://doi.org/10.1061/\(ASCE\)CF.1943-5509.0001381](https://doi.org/10.1061/(ASCE)CF.1943-5509.0001381).
- Yadav, P. and Sharan, S. (2019), "Numerical investigation of squeezing in underground hard rock mines", *Rock Mech. Rock Eng.*, **52**(4), 1211-1229. <https://doi.org/10.1007/s00603-018-1632-9>.
- Yao, W.L., Sharifzadeh, M., Yang, Z., Xu, G. and Fang, Z.G. (2019), "Assessment of fracture characteristics controlling fluid flow performance in discrete fracture networks (DFN)", *J.*

Petrol. Sci. Eng., **178**, 1104-1111.
<https://doi.org/10.1016/j.petrol.2019.04.011>.

CC